THE ASTROPHYSICAL JOURNAL, 408:L85–L88, 1993 May 10

DYNAMICAL INSTABILITY AS THE CAUSE OF THE MASSIVE OUTBURSTS IN ETA CARINAE AND OTHER LUMINOUS BLUE VARIABLES

RICHARD B. STOTHERS AND CHAO-WEN CHIN
Institute for Space Studies, NASA/Goddard Space Flight Center, 2880 Broadway, New York, NY 10025
Received 1993 January 8; accepted 1993 March 1

ABSTRACT

A new type of stellar envelope structure has been computationally discovered at very high stellar masses. The outer part of the envelope resembles a nearly detached, diffusely filled shell overlying an ultrahot surface of small radius. This structural anomaly is caused by a large iron bump occurring in the new opacities of Iglesias, Rogers, and Wilson. The new stellar models with normal metallicity encounter a strong ionization-induced dynamical instability in the outer envelope as they rapidly transit the H-R diagram after the end of central hydrogen burning. Preliminary evolutionary and hydrodynamical calculations successfully mimic the most basic observed properties of η Carinae and other very luminous blue variables. The Humphreys-Davidson sloped line in the H-R diagram, however, seems to be unrelated to these variables, but is rather the observed terminus of the main-sequence phase of evolution if convective core overshooting is insignificant.

Subject headings: convection — stars: evolution — stars: individual (η Carinae) — stars: oscillations — stars: variables: other miscellaneous

1. INTRODUCTION

The brightest nonexplosive stars in large spiral galaxies comprise a class of variables that at least once in their lives eject matter at a prodigious rate, far beyond what could be expected for a radiatively driven stellar wind. Owing to the optical thickness of the shells that these stars throw off, the actual stellar effective temperatures are uncertain, and may be hotter than indicated by the F spectral types and blue to yellow colors of the composite objects (Davidson 1987). Nevertheless, the stars' bolometric luminosities can be considered known, because the bolometric corrections of the composite objects are close to zero.

In the original classification of these variables, Hubble & Sandage (1953) noted also S Doradus in the Large Magellanic Cloud but made no mention of η Carinae, although this Galactic variable is now often regarded as the prototype of the most luminous subgroup of the luminous blue variables. Eta Car is composite and may be a multiple star; its brightest component A emits a luminosity of $\sim 2 \times 10^6\ L_\odot$ (Davidson & Humphreys 1986). Its erratic visual photometric behavior since shortly before its massive outburst in 1843 has been well documented (van Genderen & Thé 1984), although its bolometric luminosity possibly remained essentially constant (Hillier & Allen 1992). The effective temperature of η Car A in its present, near-quiescent state is probably close to $\sim 3 \times 10^4$ K (Davidson 1971; Andriesse, Donn, & Viotti 1978; Hillier & Allen 1992). Eta Car A appears, therefore, to be a hot, evolved supergiant that has lost considerable mass—a conclusion that is supported by the observed overabundances of helium and nitrogen in its surrounding nebula, the so-called "homunculus" (Davidson et al. 1986; Burgarella & Paresce 1991). Its present luminosity would suggest an initial mass of $\sim 120\ M_\odot$.

Evolutionary calculations that include massive, abrupt outflows have mimicked some of the photometric behavior of very luminous blue variables like η Car (Stothers & Chin 1983; Maeder 1983). The bolometric luminosity remains nearly constant, and the effective temperature becomes very hot as the stellar envelope shrinks rapidly in thermal readjustment after an episode of heavy mass outflow. These evolutionary calculations are purely illustrative, however, because the actual mechanism of mass loss has remained unknown (Davidson 1989).

In the present paper, we identify what is possibly the destabilizing mechanism. The source appears to be dynamical instability, induced by a subtle combination of the effects of prior stellar wind mass loss, large iron opacities, partial ionization of hydrogen and helium, and high radiation pressure. These factors operate effectively together in the stars with the highest masses.

2. STABILITY AGAINST NUCLEAR-ENERGIZED PULSATIONS

We initially decided to determine whether stars of such high mass were ever unstable toward nuclear-energized pulsations in the core. Only stellar models that are chemically homogeneous had to be considered, as even rather modest inhomogeneities induce pulsational stability (Schwarzschild & Härm 1959). Using the newly revised opacities of Iglesias, Rogers, & Wilson (1992), we repeated the linear nonadiabatic pulsational analysis of Stothers (1992), who adopted hydrogen and metal abundances by mass of $X = 0.700$–0.758 and $Z = 0.002$–0.03. It now appears likely that for $Z \geq 0.02$ all stellar masses are stable (Table 1). For completeness, the critical masses of homogeneous helium-burning models are also included in Table 1. These values are almost unchanged from before.

A peculiar new feature appeared in the structure of the outer envelope for both the hydrogen-burning and helium-burning models with $Z \geq 0.02$. When the stellar mass is sufficiently high, the fundamental radial mode of pulsation (which is the only possible unstable mode) develops a node in the displacement amplitude at a temperature where the opacity has a large iron peak near 2×10^5 K. This amplitude feature, which causes the fundamental mode to look like a first overtone, is primarily a nonadiabatic effect. Occurring close to the surface, it hardly affects the stability or adiabatic period of pulsation. It comes about because the large iron opacity peak steepens the

TABLE 1

CRITICAL MASSES FOR NUCLEAR-ENERGIZED PULSATIONAL INSTABILITY OF HOMOGENEOUS MAIN-SEQUENCE STARS

	Z			
MAIN SEQUENCE	0.03	0.02	0.004	0.002
Hydrogen-burning	>150	>150	138	97
Helium-burning	21.0	18.3	14.3	13.0

NOTE.—Masses are in solar units.

local temperature gradient, creating a very high radiation pressure relative to gas pressure, such as normally exists only within the outer atmosphere of a star. In effect, the envelope layers cooler than $\sim 5 \times 10^5$ K look almost like a detached shell surrounding an extremely hot (though enormously opaque) quasi-photosphere. However, the threshold of dynamical instability is never crossed, because there exist no cool ionization zones of the abundant elements, hydrogen and helium, in these hot envelopes (§ 3).

Accordingly, we have searched for dynamical instability in the cooler envelopes of massive stars evolved well off the main sequence.

3. DYNAMICAL INSTABILITY IN THE OUTER ENVELOPE

New evolutionary sequences of stellar models were constructed for three initial masses, $M/M_\odot = 60$, 90, and 120; and for two initial chemical compositions, $(X, Z) = (0.70, 0.03)$ and (0.756, 0.004). Opacities used were those of Iglesias et al. (1992) with an adopted 2% iron percentage among the metals. Convective core overshooting was ignored, and envelope semiconvection was calculated according to the Ledoux criterion (Stothers & Chin 1992). The ratio of mixing length to local pressure scale height in the outer convective envelope was taken to be 1.4. Radiatively driven stellar wind mass loss was included by adopting mean rates fitted to observed Galactic mass loss rates by Nieuwenhuijzen & de Jager (1990). For our metal-poor composition, these adopted rates were reduced by a factor of 5 to accord with the theoretical $Z^{0.8}$ dependence of the rate found by Leitherer, Robert, & Drissen (1992).

On the Hertzsprung-Russell (H-R) diagram, the new evolutionary tracks for the main-sequence phase extend to much lower effective temperatures than was the case with the older Los Alamos opacities. The coolest predicted effective temperatures for a normal metallicity now essentially match Humphreys & Davidson's (1979) observed red limit for very luminous stars (Fig. 1). This agreement comes about without the assumption of convective core overshooting.

After hydrogen is exhausted in the core, the star moves rapidly across the H-R diagram on a secular gravitational (Helmholtz-Kelvin) time scale. To become a red supergiant requires only ~ 6000 yr. Expansion is driven by the large iron opacities near the stellar surface. At a certain stage, however, dynamical instability is triggered in the envelope if the following conditions are met.

First, the initial stellar mass must be high, generating a bright luminosity within a very massive core.

Second, the envelope mass must be significantly reduced by stellar wind mass loss, so that the ratio of luminosity to stellar mass becomes higher than normal. This combination of factors increases the fraction, $1 - \beta$, contributed by the blackbody radiation field to the total pressure P, in accordance with

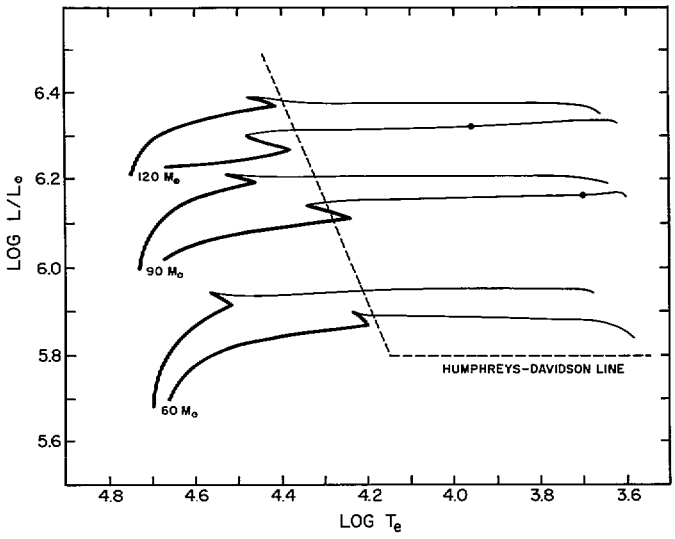

FIG. 1.—H-R diagram showing evolutionary tracks running from the zero-age main sequence to the onset of core helium burning. The slow phase of core hydrogen burning is indicated by the thick lines. Tracks are labeled with the initial stellar mass. In each dyad of tracks, the brighter track refers to $Z = 0.004$, and the fainter to $Z = 0.03$. A dot indicates the bluest stage for which dynamical instability occurs in the outer envelope; this stage, however, is very sensitive to the amount of prior mass loss (see text).

Eddington's (1921) relation

$$1 - \beta = \langle \kappa \rangle L/(4\pi cGM) , \tag{1}$$

where $\langle \kappa \rangle$ is a pressure-weighted average of the Rosseland mean opacity in the envelope. Then the first generalized adiabatic exponent Γ_1 comes close to the limit 4/3 for pure radiation pressure.

Third, Γ_1 must be reduced below 4/3 in some layers by the partial ionization of hydrogen and helium. As a result, the weighted average value of Γ_1 between the surface R and a level r,

$$\langle \Gamma_1 \rangle = \int_r^R \Gamma_1 P d(r^3) \Big/ \int_r^R P d(r^3) , \tag{2}$$

can be somewhat less than 4/3, implying the possibility of dynamical instability. In order to have actual dynamical instability, the unstable region must be effectively isolated from the rest of the star (Ledoux & Walraven 1958; Tuchman, Sack, & Barkat 1978).

A region of this type occurs in our present models at temperatures cooler than $\sim 5 \times 10^5$ K. The runs of several physical variables within the stellar envelope for a normal-metallicity model of initially 120 $M_\odot$ when it reaches $\log T_e = 3.90$ are shown in Figure 2. The selected model contains an instantaneous mass of 66.6 $M_\odot$ with surface hydrogen abundance of $X_{\rm surf} = 0.35$. Notice that the running envelope mass, $(1 - q)M$, levels off well above the quasi-photosphere at $\sim 5 \times 10^5$ K. The isolated character of this outer region of the envelope is seen better in the classical (U, V) plane, in terms of the homology invariants $U = d \ln M(r)/d \ln r$ and $V = -d \ln P/d \ln r$ (Schwarzschild 1958). Unlike the case of a simple electron-scattering envelope, which exhibits a nearly straight trajectory toward the hydrogen-burning shell, the trajectory of the present, more physically realistic envelope first develops a large loop to the left and then returns practically to its starting point (Fig. 3). This unique loop is caused entirely by the three

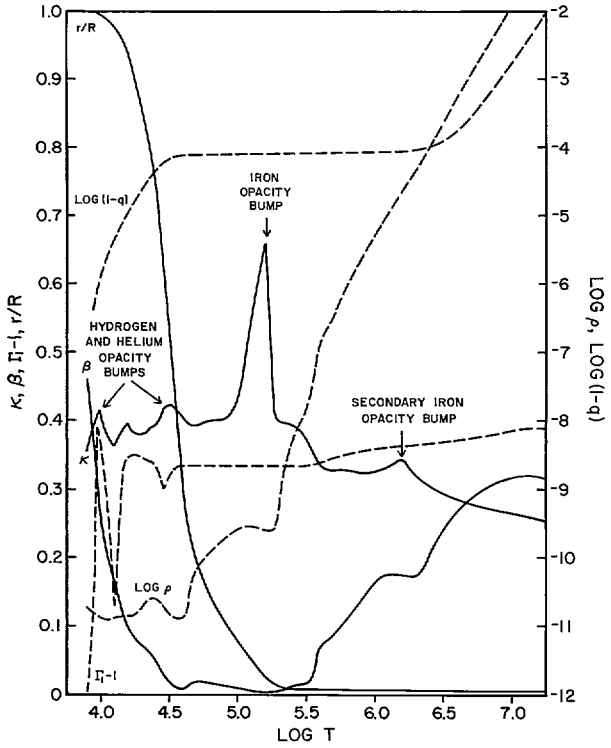

FIG. 2.—Runs of several physical variables through the envelope of a normal-metallicity star of initial 120 $M_\odot$ at a stage when $M/M_\odot = 66.6$, $X_{surf} = 0.35$, and log $T_e = 3.90$. Units of the variables are either dimensionless or cgs. The major opacity bumps are identified. The outer envelope is dynamically unstable in layers cooler than $\sim 5 \times 10^5$ K.

major opacity bumps, especially the huge iron opacity bump. (It does not occur with the smallish Cox-Stewart opacities.) Even the vigorous hydrogen-burning shell with its discontinuity in chemical composition does not come close to dividing the star into two such mechanically isolated regions.

The time history of $\langle \Gamma_1 \rangle$ in the outer envelope is displayed as a function of effective temperature in Figure 4. When $\langle \Gamma_1 \rangle$

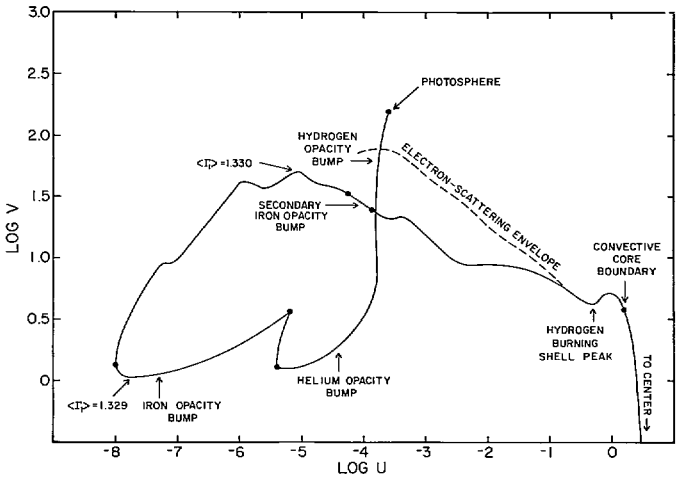

FIG. 3.—Trajectory in the (U, V) plane of the stellar model of Fig. 2. Dots identify boundaries between radiative and convective regions (follow the dots to find two iron convection zones). The trajectory for a simple electron-scattering envelope is shown for comparison.

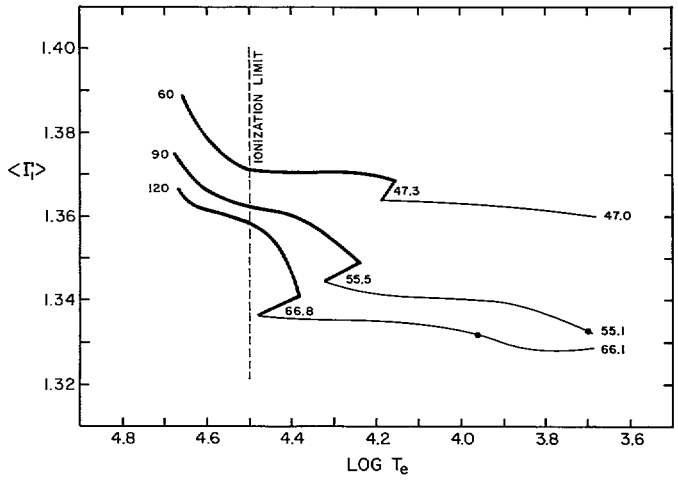

FIG. 4.—Pressure-weighted volumetric average value of the first generalized adiabatic exponent, Γ_1, in the outer envelope, as a function of effective temperature, along the three normal-metallicity evolutionary tracks of Fig. 1. Stellar masses are indicated in solar units. Thick lines refer to the slow phase of core hydrogen burning. A dot indicates the bluest stage for which dynamical instability occurs in the outer envelope.

reaches the value 4/3, the outer envelope becomes dynamically unstable. We have independently verified this hydrostatically derived result by radially perturbing the whole stellar structure in the linear adiabatic approximation. The eigenfrequency of the fundamental mode of radial pulsation becomes purely imaginary to the right of the plotted dots in Figures 1 and 4. It should be noted that this newfound dynamical instability is not triggered by a density inversion, by atmospheric turbulence, or by an excess of the star's radiative luminosity over the Eddington luminosity limit (L in eq. [1] with $\beta = 0$), which drives the density, ρ, to zero and is never attained in a radiative zone in any of our present models. In regions of high opacity, a significant fraction of the stellar heat flux is carried by turbulent convection, without the mean convective velocities anywhere becoming close to supersonic.

Dynamical instability occurs only in our models for initial masses of 90 and 120 $M_\odot$ with a normal metals abundance. This result is consistent with the observed absence of luminous blue variables in the metal-poor Small Magellanic Cloud (Wolf 1991), although small number statistics could also be a reason. The actual effective temperature at which dynamical instability occurs, however, is very sensitive to the amount of prior mass loss. In our displayed track for 120 $M_\odot$, instability sets in at log $T_e = 3.96$, but it would occur at log $T_e = 4.25$ if the prior amount of mass loss were only 10% greater. Since the adopted rates of stellar wind mass loss are uncertain by at least a factor of 2, it is conceivable that they are systematically too small and that the phase of dynamical instability always commences at high effective temperature. This possibility could account for the observed absence of very luminous stars cooler than the Humphreys-Davidson limit. Otherwise, their observed absence would be only a statistical effect due to the rapidity of evolution in this part of the H-R diagram. At lower initial masses, say down to ~ 40 $M_\odot$, most of the stellar wind mass loss would presumably take place very rapidly in the region of red supergiants before the luminous blue variable phase begins.

The weakening of stellar stability with increased mass loss implies also that once the dynamical instability begins, the

process of mass outflow will continue unabated until the star is thermally removed to the left of the ionization limit in Figure 4. This critical effective temperature, $\sim 3 \times 10^4$ K, to the left of which no significant ionization zones exist in the star, is the place where the post-outburst central stars of η Car and of other very luminous blue variables appear to lie, more or less (Davidson 1971; Humphreys 1989; Wolf 1989). When the envelope begins to re-expand after an outburst, it does so at a more rapid rate than before owing to the reduced envelope mass (Stothers & Chin 1983). This fast expansion may be what is now observed in P Cygni (Lamers & de Groot 1992). Later, another outburst must inevitably ensue at some effective temperature not far below $\sim 3 \times 10^4$ K, and the cycle is repeated until the star is permanently displaced to the left of the ionization limit.

4. MASS OUTFLOW

Our new calculations show that the amount of mass contained in the instantaneous outer envelope in its equilibrium state depends mainly on effective temperature, and only very slightly on initial stellar mass, rate of prior mass loss, or metallicity. It amounts to $\sim 10^{-4}\ M_\odot$ near the Humphreys-Davidson sloped line and $\sim 10^{-2}\ M_\odot$ in the region of red supergiants. Since the time scale for loss of this outer envelope is expected to be of the order of $10^{1\pm1}(R/v_e)$, where $v_e = (2GM/R)^{1/2}$, a reasonable estimate for the mean rate of mass outflow would be $\sim 10^{-3\pm1}\ M_\odot\ \mathrm{yr}^{-1}$. This prediction agrees in general order with the observationally derived rate of mass loss for η Car in the ~ 30 years around its great outburst in 1843, which has been estimated as $4 \times 10^{-3}\ M_\odot\ \mathrm{yr}^{-1}$ by van Genderen & Thé (1984), $2 \times 10^{-2}\ M_\odot\ \mathrm{yr}^{-1}$ (or more) by Hyland et al. (1979), $7 \times 10^{-2}\ M_\odot\ \mathrm{yr}^{-1}$ by Andriesse et al. (1978) and $\sim 10^{-1}\ M_\odot\ \mathrm{yr}^{-1}$ by Davidson (1989). Since mass loss will theoretically go on until the underlying star finally responds by shrinking, the total amount of mass lost in a single episode is predicted to be many times the mass of the instantaneous outer envelope. This qualitative expectation at least conforms with the measured mass of η Car's "homunculus," 0.1–2 $M_\odot$. Further observational support for our model includes the fact that the "homunculus" is observed to be an expanding hollow shell (Hester et al. 1991; Hillier & Allen 1992). Its extreme dustiness (Andriesse et al. 1978) and oblate, bipolar shape suggest that the envelope of η Car A is strongly magnetic. If so, the magnetic field would not significantly affect the onset of dynamical instability (Stothers 1981).

A fully nonlinear hydrodynamical calculation has been performed for one dynamically unstable envelope model of the present type. Small motions are initiated from pure white noise, and are found to develop immediately into slow relaxation oscillations of rapidly growing amplitude and lengthening period. Although the bolometric light variation is relatively small, the strong effect of bolometric correction leads to large blue and visual light variations, because the effective temperature varies as $R^{-1/2}$. Such pulsations may possibly explain η Car's three or more sharp visual brightness increases occurring at intervals of 5–10 yr before its main outburst in 1843 (van Genderen & Thé 1984). The extremely luminous Variable B in M33 also exhibited the same kind of oscillatory behavior before its 1963 outburst (Hubble & Sandage 1953; Rosino & Bianchini 1973), as did Variable 12 in NGC 2403 before its 1954 outburst (Tammann & Sandage 1968).

Further evolutionary and pulsational calculations would seem to be called for by the apparent success of the present exploratory models.

It is a pleasant duty to thank F. J. Rogers, C. A. Iglesias, and B. G. Wilson for sending us their new tables of opacities. An anonymous referee made some helpful suggestions for clarifying certain points.

REFERENCES

Andriesse, C. D., Donn, B. D., & Viotti, R. 1978, MNRAS, 185, 771
Burgarella, D., & Paresce, F. 1991, A&A, 241, 595
Davidson, K. 1971, MNRAS, 154, 415
———. 1987, ApJ, 317, 760
———. 1989, in Physics of Luminous Blue Variables, ed. K. Davidson, A. F. J. Moffat, & H. J. G. L. M. Lamers (Dordrecht: Kluwer), 101
Davidson, K., Dufour, R. J., Walborn, N. R., & Gull, T. R. 1986, ApJ, 305, 867
Davidson, K., & Humphreys, R. M. 1986, A&A, 164, L7
Eddington, A. S. 1921, Z. Phys., 7, 351
Hester, J. J., Light, R. M., Westphal, J. A., Currie, D. G., Groth, E. J., Holtzman, J. A., Lauer, T. R., & O'Neil, E. J., Jr. 1991, AJ, 102, 654
Hillier, D. J., & Allen, D. A. 1992, A&A, 262, 153
Hubble, E., & Sandage, A. 1953, ApJ, 118, 353
Humphreys, R. M. 1989, in Physics of Luminous Blue Variables, ed. K. Davidson, A. F. J. Moffat, & H. J. G. L. M. Lamers (Dordrecht: Kluwer), 3
Humphreys, R. M., & Davidson, K. 1979, ApJ, 232, 409
Hyland, A. R., Robinson, G., Mitchell, R. M., Thomas, J. A., & Becklin, E. E. 1979, ApJ, 233, 145
Iglesias, C. A., Rogers, F. J., & Wilson, B. G. 1992, ApJ, 397, 717
Lamers, H. J. G. L. M., & de Groot, M. J. H. 1992, A&A, 257, 153
Ledoux, P., & Walraven, T. 1958, in Handbuch der Physik, Vol. 51, ed. S. Flügge (Berlin: Springer), 353
Leitherer, C., Robert, C., & Drissen, L. 1992, ApJ, 401, 596
Maeder, A. 1983, A&A, 120, 113
Nieuwenhuijzen, H., & de Jager, C. 1990, A&A, 231, 134
Rosino, L., & Bianchini, A. 1973, A&A, 22, 453
Schwarzschild, M. 1958, Structure and Evolution of the Stars (Princeton: Princeton Univ. Press)
Schwarzchild, M., & Härm, R. 1959, ApJ, 129, 637
Stothers, R. B. 1981, MNRAS, 197, 351
———. 1992, ApJ, 392, 706
Stothers, R. B., & Chin, C.-w. 1983, ApJ, 264, 583
———. 1992, ApJ, 390, L33
Tammann, G. A., & Sandage, A. 1968, ApJ, 151, 825
Tuchman, Y., Sack, N., & Barkat, Z. 1978, ApJ, 219, 183
van Genderen, A. M., & Thé, P. S. 1984, Space Sci. Rev., 39, 317
Wolf, B. 1989, A&A, 217, 87
———. 1991, in IAU Symp. 148, The Magellanic Clouds, ed. R. Haynes & D. Milne (Dordrecht: Kluwer), 266